Research Article

ADVANCED PHOTONICS

Breaking the diffraction limit in molecular imaging by structured illumination mid-infrared photothermal microscopy

Pengcheng Fu,[a,†] Bo Chen,[a,†] Yongqing Zhang,[a] Liangyi Chen,[b] Hyeon Jeong Lee,[c,d,*] and Delong Zhang[a,*]

[a]Zhejiang University, School of Physics, Zhejiang Key Laboratory of Micro-nano Quantum Chips and Quantum Control, Hangzhou, China
[b]Peking University, Institute of Molecular Medicine, School of Future Technology, Peking-Tsinghua Center for Life Sciences, New Cornerstone Science Laboratory, State Key Laboratory of Membrane Biology, Beijing Key Laboratory of Cardiometabolic Molecular Medicine, Beijing Laboratory of Biomedical Imaging, Beijing, China
[c]Zhejiang University, College of Biomedical Engineering and Instrument Science, Key Laboratory for Biomedical Engineering of Ministry of Education, Hangzhou, China
[d]Zhejiang University, MOE Frontier Science Center for Brain Science & Brain-Machine Integration, Hangzhou, China

Abstract. Super-resolution microscopy techniques have revolutionized biological imaging by breaking the optical diffraction limit, yet most methods rely on fluorescent labels that provide limited chemical information. Although vibrational imaging based on Raman and infrared (IR) spectroscopy offers intrinsic molecular contrast, achieving both high spatial resolution and high chemical specificity remains challenging due to weak signal levels. We demonstrate structured illumination mid-infrared photothermal microscopy (SIMIP) as an emerging imaging platform that provides chemical bond selectivity and high-speed, widefield detection beyond the diffraction limit. By modulating fluorescence quantum yield through vibrational infrared absorption, SIMIP enables both nanoscale spatial resolution and high-fidelity IR spectral acquisition. The synergy of enhanced resolution and chemical specificity positions SIMIP as a versatile tool for studying complex biological systems and advanced materials, offering new opportunities across biomedicine and materials science.

Keywords: structured illumination microscopy; vibrational imaging; fluorescence readout; mid-infrared photothermal microscopy.

Received Dec. 2, 2024; revised manuscript received Feb. 28, 2025; accepted for publication Mar. 10, 2025; published online Apr. 13, 2025.

[DOI: 10.1117/1.AP.7.3.036003]

1 Introduction

Optical imaging has transformed numerous scientific disciplines by providing new insights into the mechanisms of nature. Advances in resolving power have enabled deeper insights, wherein single-molecule fluorescence techniques have emerged as a dominant approach for probing the sub-ten nanometer range. Although super-resolution techniques have found many successes, they are mostly limited to protein-specific fluorophores and dyes, presenting challenges in targeting small molecules. To directly obtain molecular information beyond fluorescent labels, vibrational spectroscopy and imaging have emerged as powerful alternatives. Notably, due to their interactions with intrinsic molecular bond vibrations, vibrational spectroscopy and microscopy have gained increasing popularity for their unique advantages, enabling the extraction of chemical information without the need for extensive sample processing or labeling.[1–3]

Recent decades have witnessed rapid advances in vibrational photothermal imaging methods that detect physical changes induced by vibrational infrared (IR) absorption. These techniques include photothermal lensing, also known as mid-infrared photothermal (MIP) or O-PTIR microscopy,[4,5] which probes modulations in local refractive index; photoacoustic imaging,[6,7] which measures temperature-dependent variations in acoustic

*Address all correspondence to Hyeon Jeong Lee, hjlee@zju.edu.cn; Delong Zhang, dlzhang@zju.edu.cn

†These authors contributed equally to this work.

signals; quantitative phase imaging,[8,9] which captures changes in optical path length; and optical coherence tomography,[10] which detects interferometric variations. By leveraging visible light detection, these methods achieve spatial resolution far beyond the diffraction limit of conventional IR imaging while maintaining their chemical specificity through vibrational absorption.

Notably, breaking the diffraction limit has remained challenging for vibrational spectroscopy techniques, which exhibit much weaker interactions with typical Raman scattering cross-sections of 10^{-30} cm^2 and IR absorption cross-sections of 10^{-21} cm^2 compared to the fluorescence cross-sections of 10^{-16} cm^2. Despite advancements such as synthetic aperture,[11] high-order harmonic lock-in detection,[5] saturation effects,[12] and photoswitchable Raman probe,[13] the inherently weak signal levels preclude the direct application of advanced single-molecule-based fluorescence super-resolution approaches. To address this challenge, significant efforts have focused on utilizing highly sensitive fluorescence methods with vibrational spectroscopy techniques, specifically fluorescence-enhanced mid-infrared photothermal microscopy (F-MIP, or F-PTIR).[14,15] Compared with the temperature-modulated refractive index changes in conventional MIP,[4] fluorescence emission efficiency is significantly more responsive to temperature modulation,[16–18] offering various possibilities in high-sensitivity chemical imaging as a readout method.

However, not all fluorescence-based super-resolution techniques[19–24] can be readily employed by vibrational photothermal methods to break the diffraction limit. For example, single-molecule localization methods, such as PALM[20] or STORM,[24] would have difficulty in detecting local heating-induced changes in the fluorescence quantum yield of a single molecule. Meanwhile, STED-type detection employs a quenching donut beam, which inevitably induces local heating due to fluorescence quenching, obscuring the subtle heating effects caused by IR pulses.

By contrast, structured illumination microscopy (SIM)[25,26] presents significant potential for MIP as an effective and sensitive readout method. SIM exploits the Moiré effect to translate the otherwise inaccessible high-frequency spatial information into a detectable low-frequency range through the superposition of a fine pattern generated by the controlled interference of coherent light beams. Current SIM technology can achieve rapid readouts of hundreds of frames with high-throughput widefield imaging capability,[27–29] making it a promising candidate for high-speed vibrational imaging beyond the diffraction limit.[30]

Here, we introduce structured illumination mid-infrared photothermal microscopy (SIMIP), a novel high-speed vibrational imaging approach that breaks the diffraction limit. SIMIP overcomes the traditional speed-resolution tradeoff that has limited vibrational imaging techniques by leveraging the ability of structured illumination to encode high-frequency spatial information into detectable low-frequency patterns. The synchronized widefield detection of IR-modulated fluorescence enables simultaneous capture of both spatial features that are below the diffraction limit and bond-specific chemical contrast, extracting rich molecular information across the entire field of view. The innovation of SIMIP lies in its unique combination of capabilities from distinct physical processes and image reconstruction: (1) it harnesses the sensitivity of fluorescence-based detection for vibrational signatures, (2) breaks diffraction limit through structured illumination in a widefield configuration, and (3) employs sophisticated reconstruction algorithms to push spatial resolution beyond the diffraction limit. The synergy of these capabilities positions SIMIP as a powerful tool for diverse applications across biomedicine and materials science.

2 Results

2.1 Principle of SIMIP

SIMIP breaks the diffraction limit by utilizing the moiré effect within the SIM framework (Fig. 1). Briefly, the underlying physics of SIM can be understood through reciprocal space analysis, where the conventional optical transfer function (OTF) defines a hard boundary for detectable spatial frequencies. By applying structured illumination patterns with varying phases [Figs. 1(a) and 1(b)], high-frequency information is downshifted into detectable low-frequency ranges along the axis perpendicular to the illumination pattern. By systematically rotating the

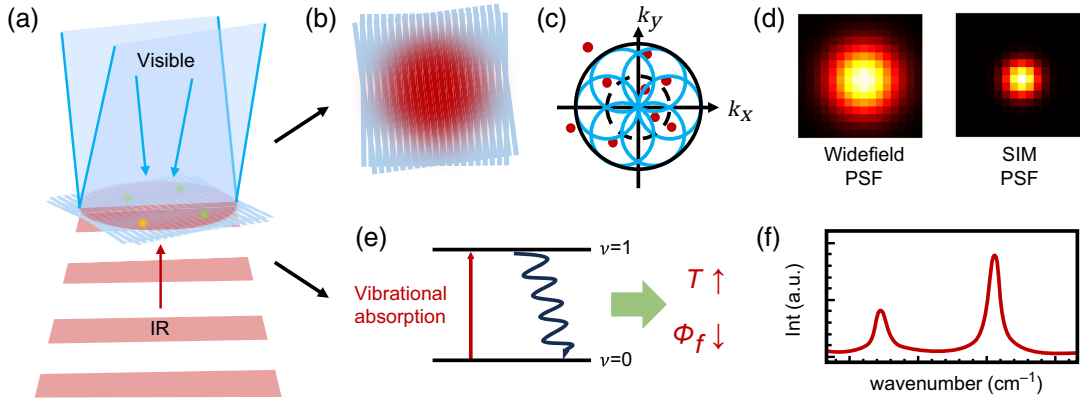

Fig. 1 Principle of SIMIP. (a) Schematic of the SIMIP system. (b) Schematic diagram of illumination pattern on the imaging plane. (c) Isotropic extension of OTF by varying the phase and the orientation of the illumination pattern. The red dot represents the projection of the sample in the reciprocal space. (d) Simulated PSF for widefield imaging and SIM imaging, respectively. (e) Modulation of the fluorophore emission intensity by the IR pulse vibrational absorption of nearby molecules. (f) Chemical information obtained using SIMIP.

orientation of these stripe patterns, an enhanced isotropic resolution is achieved through frequency space expansion [Fig. 1(c)]. Consequently, the use of structured illumination narrows the point spread function (PSF) of the system, breaking the diffraction limit by two times[26] [Fig. 1(d)].

SIMIP utilizes the MIP effect to access molecular-specific information. A pulsed IR pump beam is used to selectively excite specific molecular bonds through vibrational absorption followed by nonradiative relaxation from the excited molecules [Fig. 1(e)], which generates localized heating (increasing T) and reduces the quantum yield of nearby fluorophores (decreasing Φ). Through comparative analysis of SIM images acquired with and without bond-selective heating across varying IR wavelengths, IR spectral response at each pixel can be obtained [Fig. 1(f)]. Importantly, because SIMIP signals are derived from paired SIM images, the spatial resolution achieved matches that of conventional SIM imaging.

2.2 SIMIP Development

SIMIP implementation is remarkably straightforward, requiring minimal modifications to existing commercial SIM systems by introducing a mid-infrared laser beam in the counter-propagating configuration [Fig. 2(a)]. For mid-infrared excitation, a quantum cascade laser (QCL, MIRcat, Daylight Solutions) at 500 kHz with 300 ns pulses induces transient thermal modulation of fluorophore quantum yield. Ideally, the IR pulse and probe pulse with proper durations should be synchronized to ensure maximum temperature modulation for fluorescence readout and avoid extensive thermal dissipation to maintain the best resolution.[31] The QCL beam is weakly focused at the sample plane to match the large field of view. The optical configuration comprises a 488-nm continuous-wave laser delivered through a single-mode fiber into free space. The laser is sent through a polarizing beam splitter into a spatial light modulator (SLM) that generates structured illumination patterns by diffracting the incident beam into $\pm$1st orders while blocking the 0th order with a mask. The SLM modulates these patterns with varying phases and orientations at kilohertz frequencies. A multiband dichroic mirror was incorporated into the optical path to direct the excitation beam and effectively separate the emitted fluorescence from the excitation beam.

Fluorescence signals are collected through the objective lens and captured by an sCMOS camera, whereas real-time display and control are accomplished using a ZYNQ embedded system platform that integrates an ARM processor with FPGA-based programmable logic. HIS-SIM system used in this study incorporates advanced data processing algorithms, namely Hessian SIM and sparse deconvolution.[28,29] Hessian SIM uses the Hessian matrix and prior knowledge of biological structure continuity across dimensions to reconstruct SIM images with less than 10% of the photon dose required by conventional SIM.[28] Sparse deconvolution, utilizing the sparsity and continuity of biological structures, enables HIS-SIM to achieve a maximum spatial resolution of ~60 nm while supporting real-time super-resolution imaging at rates exceeding 24 Hz.[29] The effectiveness of SIM technology relies not only on optical devices but also on advanced algorithms for post-processing acquired data, which enhance spatial resolution, enabling computational super-resolution. Several algorithms have been optimized to improve data processing speed and imaging resolution.[28,29,32–34]

The system operates by synchronizing IR pump pulses with SIM acquisition [Figs. 2(b) and 2(c)] to obtain paired "hot" (IR-on) and "cold" (IR-off) images. Each state requires nine raw image pairs under different structured illumination configurations for complete reconstruction (Fig. S1 in the Supplementary Material). The sCMOS exposure time for raw image acquisition is 30 ms per reconstructed SIM image, whereas the IR pulse duration is 80 ms to ensure continuous irradiation during hot image capture. Due to the temperature-dependent modulation of fluorescence emission efficiency, the fluorescence intensity in the hot image is weaker than that in the cold image when vibrational absorption occurs. Subtracting the hot image from the cold image yields the SIMIP image (Fig. S2 in the Supplementary Material).

2.3 SIMIP Performance Validation: Spectral Fidelity

To test the spectral fidelity of SIMIP, we employed 200-nm polymethyl methacrylate (PMMA) beads (UFPA0102G, Wuxi Rigor Technology) uniformly doped with thermosensitive

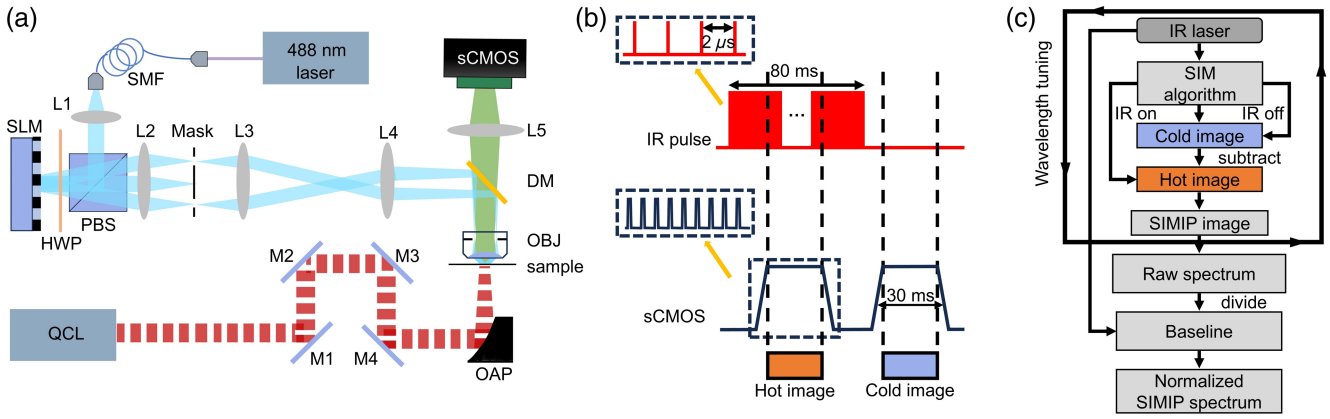

Fig. 2 Setup and data acquisition process of SIMIP. (a) Setup of SIMIP. SMF, single-mode fiber; SLM, spatial light modulator; HWP, half-wave plate; PBS, polarizing beam splitter; L, lens; M, mirrors; OAP, off-axis parabolic mirror; OBJ, objective; DM, dichroic mirror; sCMOS, scientific complementary metal-oxide semiconductor; QCL, quantum cascade laser. (b) The time scheme of SIMIP. (c) The process of obtaining SIMIP spectra.

fluorescent dyes [nitrobenzoxadiazole-based (NBD-based) fluorescent dye] as a model system. Sample preparation can be found in Note 1 of the Supplementary Material. SIMIP spectra were acquired by sweeping the QCL across $1420-1778\ \mathrm{cm}^{-1}$ range at $1\ \mathrm{cm}^{-1}$ intervals and collecting SIMIP images at each wavelength [Figs. 3(a)–3(d), Fig. S3 in the Supplementary Material]. The SIMIP spectrum was averaged 6 times, normalized by the power spectrum of QCL measured, and compared with reference spectra obtained through conventional FTIR spectroscopy (iS50R, NICOLET, with $4\ \mathrm{cm}^{-1}$ spectral resolution) [Fig. 3(b)]. The observed spectra are in good agreement in both peak positions and relative intensities throughout the fingerprint region, demonstrating the capability of SIMIP to reproduce the chemical bond information as traditional spectroscopic techniques. SIMIP images display varying responses at different wavenumbers, illustrating the spectral selectivity [Figs. 3(c) and 3(d)]. From the raw fluorescence signal traces after baseline correction, we observed signal fluctuations of up to 26% (Fig. S3 in the Supplementary Material), demonstrating a substantial photothermal modulation depth. Nevertheless, this effect is primarily attributable to heat accumulation in the larger beads (Fig. S4 in the Supplementary Material), which results from suboptimal temporal synchronization. This limitation can be effectively addressed through enhanced electronic control systems in future implementations. Based on these measurements and typical $\mathrm{d}\Phi/\mathrm{d}T$ of ~1% per Kelvin for common fluorophores,[14,15,35] we estimate that these 2-μm polymer beads in air experienced a temperature rise of ~20 K.

2.4 Resolution Enhancement of SIMIP

To quantitatively evaluate the resolution enhancement by SIMIP, we conducted comparative imaging studies using 200 nm PMMA beads uniformly labeled with fluorescent molecules. Initial SIMIP imaging at the carboxyl C=O band ($1730\ \mathrm{cm}^{-1}$) demonstrated successful chemical imaging beyond the diffraction limit [Fig. 3(e)]. Direct comparisons between SIMIP and conventional F-MIP/F-PTIR were performed on identical fields of view [Figs. 3(e) and 3(f)], with resolution quantified through intensity profile analysis across single beads [Fig. 3(g)]. The F-MIP/F-PTIR images were obtained from unprocessed data from the same microscope, without structured illumination and image processing. The measured full width at half maximum (FWHM) values were 335 nm for SIMIP and 444 nm for F-MIP/F-PTIR. After deconvolution with the known bead diameter (200 nm), we determined true spatial resolutions of 269 and 397 nm for SIMIP and F-MIP/F-PTIR, respectively. This ~1.5-fold resolution enhancement is particularly evident in the analysis of closely spaced beads [Fig. 3(h)], where SIMIP clearly resolved adjacent structures that remain ambiguous under F-MIP/F-PTIR. Although the resolution

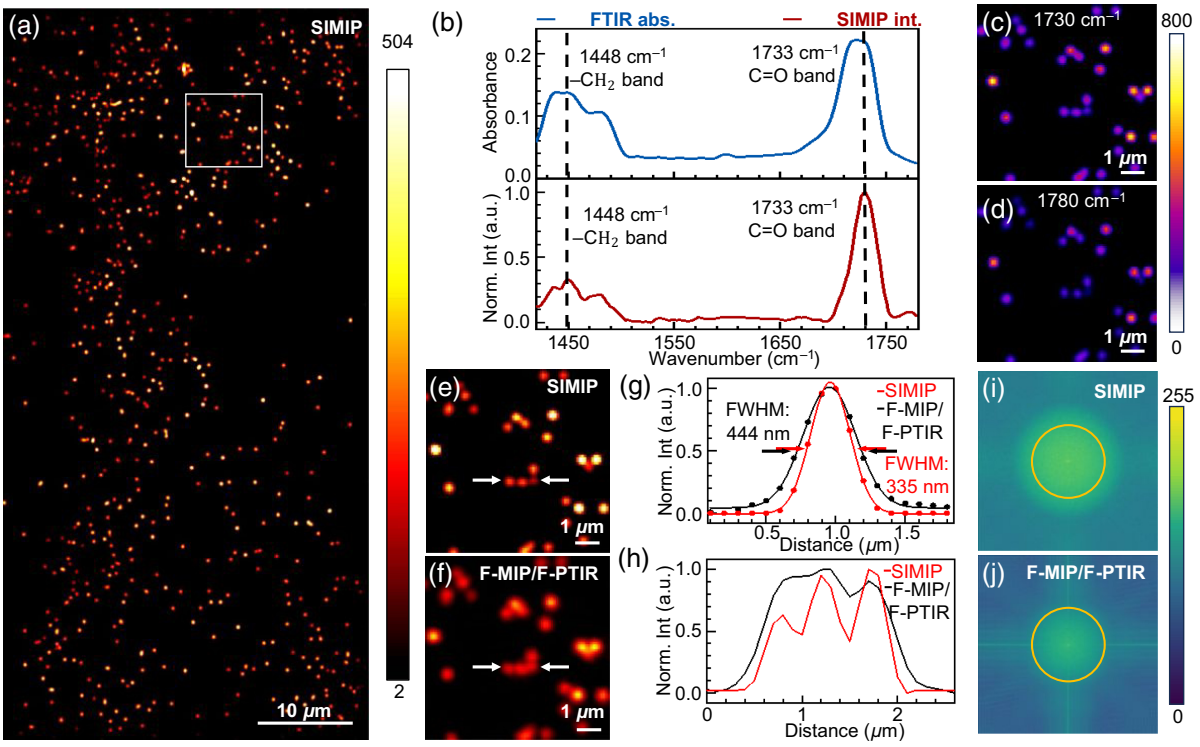

Fig. 3 SIMIP imaging performance. (a) SIMIP images of 200-nm PMMA beads at $1730\ \mathrm{cm}^{-1}$. (b) Spectra of PMMA film measured by FTIR (blue) and PMMA beads measured by SIMIP (red). int., intensity; abs. absorption; a.u., arbitrary units. (c), (d) SIMIP images of 200-nm PMMA beads at different wavenumbers. (e), (f) The enlarged images of the selected region in panel (a) using SIMIP (e) and F-MIP/F-PTIR (f), respectively. (g) The intensity profiles of a single bead using SIMIP (red) and F-MIP/F-PTIR (black), respectively. (h) The intensity profiles of the PMMA beads images indicated by the white arrows in panels (e) and (f). (i), (j) The frequency domain amplitude images of the same beads using SIMIP (i) and F-MIP/F-PTIR (j). The yellow boxes in panels (i) and (j) highlight the same region.

of F-MIP/F-PTIR approaches its theoretical limit, SIMIP successfully overcomes this barrier through structured illumination. Nonetheless, the current SIMIP still has room for improvement, as the theoretical SIM resolution improvement is twofold. It is due to a magnification mismatch in the current system using a long working distance objective lens for the convenience of prototyping (Fig. S5, Note 2 in the Supplementary Material). The uniform distribution of fluorophores throughout the microspheres ensures accurate co-localization between chemical and spatial information, validating the fidelity of our resolution measurements.

To quantitatively assess the OTF extension capability, full images of both SIMIP and F-MIP/F-PTIR were selected for FFT analysis [Figs. 3(i) and 3(j)]. The resulting FFT distribution in SIMIP exhibited a notably broader spread beyond the reference boundary (yellow circle) compared with the F-MIP/F-PTIR map, demonstrating enhanced capability in capturing high-frequency spatial information using SIMIP.

2.5 Chemical Differentiation Beyond the Diffraction Limit

To demonstrate the ability to obtain sub-diffraction limited imaging with simultaneous chemical contrast using SIMIP, we analyzed a mixture of 200-nm fluorescent polystyrene (PS) beads (UFPS0102G, Wuxi Rigor Technology) and PMMA beads (UFPA0102G, Wuxi Rigor Technology). Despite being labeled with identical fluorescent dyes, these materials exhibit distinct vibrational signatures in their fingerprint regions, making them ideal candidates for testing the chemical discrimination capabilities of SIMIP. Conventional fluorescence microscopy [Fig. 4(a)] fails to differentiate between PS and PMMA beads, with apparent "single" beads often representing unresolved aggregates.

By contrast, SIMIP imaging [Fig. 4(b)] not only resolves individual beads within these aggregates but also distinguishes their chemical composition through multi-wavelength vibrational imaging [Figs. 4(c)–4(f)]. This dual enhancement in spatial resolution and chemical selectivity demonstrates the unique ability of SIMIP to reveal molecular heterogeneity at the sub-diffraction scale, a capability beyond traditional fluorescence microscopy.

3 Discussion

SIMIP extends the established capabilities of conventional SIM into new frontiers of chemical imaging. Although SIM has

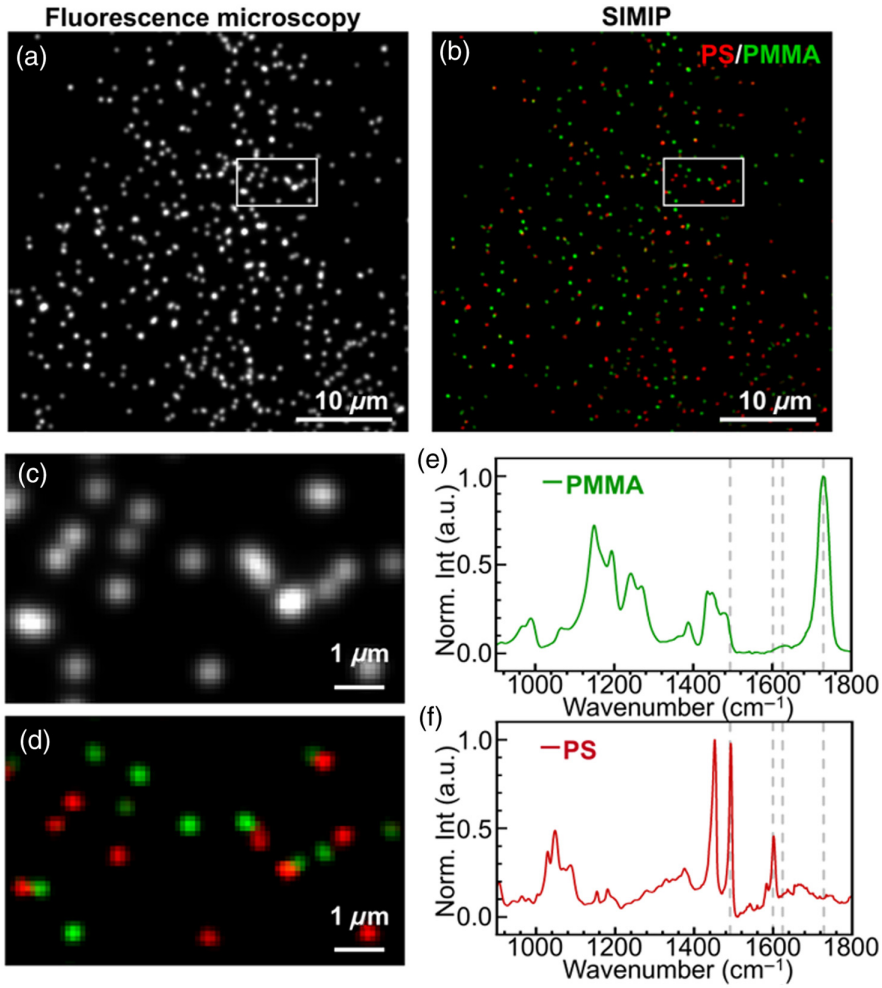

Fig. 4 Fluorescence and SIMIP images of the mixture of PS beads and PMMA beads. (a), (b) Fluorescence (a) and SIMIP (b) images from the same position in the sample. (c), (d) The enlarged images of the selected region in panels (a) and (b). (e), (f) Standard FTIR spectra of PS (e) and PMMA samples (f), respectively. Vertical lines indicate the selected wavelengths.

proven invaluable in elucidating complex cellular architectures, including extracellular vesicles (EVs),[36] platelet ultrastructure,[37] cytoskeletal organization,[38] synaptic and dendritic morphology in neurons,[39] and bacterial dynamics,[40] SIMIP introduces an additional dimension of chemical specificity. This integration could enable the detection of small-molecule metabolites and their interactions with these biological structures at unprecedented resolution. Despite the aqueous environment of living systems reducing temperature increase and accelerating cooling through higher heat capacity and thermal conductivity, the SIMIP signal can be compensated by appropriately shortening the pump pulse duration and adopting a pulsed probe.[41] Nonetheless, the fluorescence detection approach maintains higher sensitivity compared with conventional photothermal methods.[14,15] This advancement could reveal new insights into metabolite distributions and their functional relationships with cellular architecture, potentially transforming our understanding of cellular biochemistry at the nanoscale.

It is worth noting that the term SIM is most frequently referred to by default as a branch of fluorescence microscopy, although structured illumination strategies have also been used in imaging and sensing outside the fluorescence community. Structured illumination for coherent detection imaging is generally not considered to break the diffraction limit, as discussed in previous literature.[42] Nonetheless, in fluorescence microscopy, SIM acts as an excitation source to enhance the emission at a new wavelength, enabling a 2× improvement with up to 60-nm lateral resolution when implemented with proper algorithms,[29] which exceeds the conventional diffraction limit for fluorescence imaging.

Although fluorescence imaging is mostly considered a labeling technique, recent development of label-free techniques based on autofluorescence has shown promise by minimizing potential perturbation and enabling non-invasive detection. The SIMIP system by design is compatible with autofluorescence detection, requiring only a simple modification to the optical setup: converting the widefield SIM into a point-scanning SIM to enable structured excitation of autofluorescence. For example, autofluorescence-detected photothermal infrared spectroscopy is demonstrated to characterize temperature changes without the use of exogenous fluorescent reporters,[43] in which infrared-induced temperature change modulates the two-photon excited autofluorescence. Furthermore, a widefield photothermal detection method using autofluorescence has been proposed, which employs a shorter-wavelength probe beam and offers good instrumentation compatibility.[44]

Although vibrational imaging techniques employing fluorescence detection have emerged, such as bond-selective fluorescence-detected infrared-excited (BonFIRE) microscopy and stimulated Raman-excited fluorescence (SREF),[45,46] SIMIP represents a fundamentally distinct approach. Although these methods share an IR pump and fluorescence readout scheme, SREF/BonFIRE rely on exogenous fluorophores and are limited to detecting the intrinsic vibrational signatures of the fluorescent molecules themselves. By contrast, SIMIP derives its signal from fluorescence intensity modulations induced by IR absorption of neighboring molecules, offering substantially greater flexibility in target molecule selection. This key distinction enables SIMIP to probe a broader range of molecular species without being constrained by the spectroscopic properties of the fluorophore.

Nonetheless, the current SIMIP system holds significant potential for improving imaging speed. The current limitation primarily comes from the closed architecture of the commercial SIM system for slow modulation of the QCL pulse train. Future optimizations will focus on the comprehensive integration of the master clock for precise synchronization of the exposure window of the camera with the pulsed pump and pulsed probe, enabling interlaced hot- and cold-frame acquisition at kilohertz frequencies.[41,47] Implementation of this high-speed synchronization strategy could dramatically accelerate imaging rates to achieve video-rate capture or even hundreds of frames per second.

In summary, we have developed SIMIP, a chemical imaging platform beyond the diffraction limit, by exploiting the high sensitivity and resolving power of fluorescence detection with vibrational photothermal spectroscopy. SIMIP exploits temperature-dependent fluorescence modulation to overcome the traditionally weak signals in vibrational imaging. We have validated both the spectral fidelity and enhanced spatial resolution of SIMIP, demonstrating its capability to differentiate chemical species at the nanoscale. Future advancements in SIMIP will benefit from the continued development of SIM reconstruction algorithms and the use of higher temperature-sensitive fluorophores.[48,49]

Disclosures

The authors declare no conflicts of interest.

Code and Data Availability

The data and code supporting this study are available from the corresponding authors upon reasonable request.

Acknowledgments

This project is supported by the National Key Research and Development Program of China (Grant No. 2024YFA1408900), the National Natural Science Foundation of China (Grant Nos. 82372011 and 12074339), the Zhejiang Provincial Natural Science Foundation (Grant No. LZ25H180001), and the Fundamental Research Funds for the Central Universities (Grant No. 2025ZFJH01-01).

References

1. Y. Zhang et al., "Spatial sterol metabolism unveiled by stimulated Raman imaging," *Front. Chem.* **11**, 1166313 (2023).
2. J. Chen et al., "Chemical morphology of Areca nut characterized directly by Fourier transform near-infrared and mid-infrared microspectroscopic imaging in reflection modes," *Food Chem.* **212**, 469–475 (2016).
3. D. Zhang et al., "Quantitative vibrational imaging by hyperspectral stimulated Raman scattering microscopy and multivariate curve resolution analysis," *Anal. Chem.* **85**, 98–106 (2012).
4. D. Zhang et al., "Depth-resolved mid-infrared photothermal imaging of living cells and organisms with submicrometer spatial resolution," *Sci. Adv.* **2**, e1600521 (2016).
5. P. Fu et al., "Super-resolution imaging of non-fluorescent molecules by photothermal relaxation localization microscopy," *Nat. Photonics* **17**, 330–337 (2023).
6. J. Shi et al., "High-resolution, high-contrast mid-infrared imaging of fresh biological samples with ultraviolet-localized photoacoustic microscopy," *Nat. Photonics* **13**, 609–615 (2019).
7. M. A. Pleitez et al., "Label-free metabolic imaging by mid-infrared optoacoustic microscopy in living cells," *Nat. Biotechnol.* **38**, 293–296 (2019).

8. D. Zhang et al., "Bond-selective transient phase imaging via sensing of the infrared photothermal effect," *Light Sci. Appl.* **8**, 116 (2019).
9. K. Toda et al., "Adaptive dynamic range shift (ADRIFT) quantitative phase imaging," *Light Sci. Appl.* **10**, 1 (2021).
10. M. Tamamitsu et al., "Label-free biochemical quantitative phase imaging with mid-infrared photothermal effect," *Optica* **7**, 359–366 (2020).
11. M. Tamamitsu et al., "Mid-infrared wide-field nanoscopy," *Nat. Photonics* **18**, 738–743 (2024).
12. L. Gong et al., "Saturated stimulated-Raman-scattering microscopy for far-field superresolution vibrational imaging," *Phys. Rev. Appl.* **11**, 034041 (2019).
13. J. Shou et al., "Super-resolution vibrational imaging based on photoswitchable Raman probe," *Sci. Adv.* **9**, eade9118 (2023).
14. Y. Zhang et al., "Fluorescence-detected mid-infrared photothermal microscopy," *J. Am. Chem. Soc.* **143**, 11490–11499 (2021).
15. M. Li et al., "Fluorescence-detected mid-infrared photothermal microscopy," *J. Am. Chem. Soc.* **143**, 10809–10815 (2021).
16. D. Chretien et al., "Mitochondria are physiologically maintained at close to 50°C," *PLoS Biol.* **16**, e2003992 (2018).
17. G. Abbate et al., "The temperature dependence of the refractive index of water," *J. Phys. D: Appl. Phys.* **11**, 1167–1172 (1978).
18. H. H. Li, "Refractive index of silicon and germanium and its wavelength and temperature derivatives," *J. Phys. Chem. Ref. Data* **9**, 561–658 (1980).
19. F. Balzarotti et al., "Nanometer resolution imaging and tracking of fluorescent molecules with minimal photon fluxes," *Science* **355**, 606–612 (2016).
20. E. Betzig et al., "Imaging intracellular fluorescent proteins at nanometer resolution," *Science* **313**, 1642–1645 (2006).
21. S. W. Hell and J. Wichmann, "Breaking the diffraction resolution limit by stimulated emission: stimulated-emission-depletion fluorescence microscopy," *Opt. Lett.* **19**, 780–782 (1994).
22. M. Hofmann et al., "Breaking the diffraction barrier in fluorescence microscopy at low light intensities by using reversibly photoswitchable proteins," *Proc. Natl. Acad. Sci. U. S. A.* **102**, 17565–17569 (2005).
23. S. T. Hess et al., "Ultra-high resolution imaging by fluorescence photoactivation localization microscopy," *Biophys. J.* **91**, 4258–4272 (2006).
24. M. J. Rust et al., "Sub-diffraction-limit imaging by stochastic optical reconstruction microscopy (STORM)," *Nat. Methods* **3**, 793–796 (2006).
25. W. Lukosz and M. Marchand, "Optischen Abbildung Unter Überschreitung der Beugungsbedingten Auflösungsgrenze," *Optica Acta: Int. J. Opt.* **10**, 241–255 (1963).
26. M. G. L. Gustafsson, "Surpassing the lateral resolution limit by a factor of two using structured illumination microscopy," *J. Microsc.* **198**, 82–87 (2001).
27. Y. Guo et al., "Visualizing intracellular organelle and cytoskeletal interactions at nanoscale resolution on millisecond timescales," *Cell* **175**, 1430–1442 (2018).
28. X. Huang et al., "Fast, long-term, super-resolution imaging with Hessian structured illumination microscopy," *Nat. Biotechnol.* **36**, 451–459 (2018).
29. W. Zhao et al., "Sparse deconvolution improves the resolution of live-cell super-resolution fluorescence microscopy," *Nat. Biotechnol.* **40**, 606–617 (2021).
30. K. Watanabe et al., "Structured line illumination Raman microscopy," *Nat. Commun.* **6**, 10095 (2015).
31. Y. Bai et al., "Bond-selective imaging by optically sensing the mid-infrared photothermal effect," *Sci. Adv.* **7**, eabg1559 (2021).
32. S. Tu et al., "Fast reconstruction algorithm for structured illumination microscopy," *Opt. Lett.* **45**, 1567–1570 (2020).
33. C. S. Smith et al., "Structured illumination microscopy with noise-controlled image reconstructions," *Nat. Methods* **18**, 821–828 (2021).
34. Z. Wang et al., "High-speed image reconstruction for optically sectioned, super-resolution structured illumination microscopy," *Adv. Photonics* **4**, 026003 (2022).
35. W.-C. Chen et al., "The development and application of two-color pressure-sensitive paint in jet impingement experiments," *Aerospace* **10**, 805 (2023).
36. G. Li et al., "The M2 macrophages derived migrasomes from the surface of titania nanotubes array as a new concept for enhancing osteogenesis," *Adv. Healthcare Mater.* **13**, 2400257 (2024).
37. P. Xu et al., "Superresolution fluorescence microscopy of platelet subcellular structures as a potential tumor liquid biopsy," *Small Methods* **7**, 2300445 (2023).
38. D. Li et al., "Extended-resolution structured illumination imaging of endocytic and cytoskeletal dynamics," *Science* **349**, aab3500 (2015).
39. Y. Kashiwagi et al., "Computational geometry analysis of dendritic spines by structured illumination microscopy," *Nat. Commun.* **10**, 1285 (2019).
40. L. Turnbull et al., "Super-resolution imaging of the cytokinetic Z ring in live bacteria using fast 3D-structured illumination microscopy (f3D-SIM)," *J. Vis. Exp.* 51469 (2014).
41. G. Ishigane et al., "Label-free mid-infrared photothermal live-cell imaging beyond video rate," *Light Sci. Appl.* **12**, 174 (2023).
42. K. Wicker and R. Heintzmann, "Resolving a misconception about structured illumination," *Nat. Photonics* **8**, 342–344 (2014).
43. A. Razumtcev et al., "Label-free autofluorescence-detected mid-infrared photothermal microscopy of pharmaceutical materials," *Anal. Chem.* **94**, 6512–6520 (2022).
44. C. B. Prater et al., "Widefield super-resolution infrared spectroscopy and imaging of autofluorescent biological materials and photosynthetic microorganisms using fluorescence detected photothermal infrared (FL-PTIR)," *Appl. Spectrosc.* **78**, 1208–1219 (2024).
45. H. Wang et al., "Bond-selective fluorescence imaging with single-molecule sensitivity," *Nat. Photonics* **17**, 846–855 (2023).
46. H. Xiong et al., "Stimulated Raman excited fluorescence spectroscopy and imaging," *Nat. Photonics* **13**, 412–417 (2019).
47. Y. Bai et al., "Ultrafast chemical imaging by widefield photothermal sensing of infrared absorption," *Sci. Adv.* **5**, eaav7127 (2019).
48. J. Zhou et al., "Advances and challenges for fluorescence nanothermometry," *Nat. Methods* **17**, 967–980 (2020).
49. S. Kiyonaka et al., "Genetically encoded fluorescent thermosensors visualize subcellular thermoregulation in living cells," *Nat. Methods* **10**, 1232–1238 (2013).

Pengcheng Fu is a PhD candidate in the School of Physics at Zhejiang University. He obtained his BS degree from Zhejiang University in 2020. His research focuses on vibrational microscopy, photothermal microscopy, and stimulated Raman scattering microscopy.

Bo Chen is currently a PhD candidate in the School of Physics at Zhejiang University. He received his BS degree from Zhejiang University in 2022. His research interests include stimulated Raman scattering microscopy and IR spectroscopy.

Yongqing Zhang is currently a PhD candidate in the School of Physics at Zhejiang University. He received his BS degree from the School of Physics at Zhejiang University. His research focuses on stimulated Raman scattering microscopy and its applications.

Liangyi Chen is a Boya Professor at Peking University and earned a BS/PhD in biomedical engineering from Xi'an Jiaotong University and Huazhong University of Science and Technology, respectively. His innovations include miniaturized multiphoton microscopes, Hessian-SIM, SR-FACT, and a sparse deconvolution algorithm, enabling universal super-resolution with minimal photons and overcoming optical limits. His work, featured in *Nature Methods*' 2018 Method of the Year, China's Top 10 Optics Achievements (2018), and National "13th Five-Year Plan" Innovation Exhibitions.

Hyeon Jeong Lee is an assistant professor at Zhejiang University. She received her PhD from Purdue University, and worked as a postdoctoral associate at Photonics Center of Boston University. Her research interest centers on the development and application of biophotonic techniques for functional imaging and modulation at the subcellular level to decipher the molecular machinery of life. She was listed among the 2021 MIT Technology Review Innovators Under 35 Asia Pacific and recognized in 2022 as Optica Ambassador.

Delong Zhang is a ZJU-100 professor in the School of Physics at Zhejiang University and Optica senior member. His research in molecular spectroscopy and imaging has resulted in 40 SCI papers published in journals including *Nature Photonics* and *Science Advances*, three book chapters, and eight granted patents, totaling over 3000 citations. His innovations have earned recognition through the SPIE Community Champion Award, Microscopy Today Innovation Award, and featured coverage in *Nature Photonics* News & Views.